Acta Pharmaceutica Sinica B 2022;12(5):2300–2314

Chinese Pharmaceutical Association
Institute of Materia Medica, Chinese Academy of Medical Sciences

Acta Pharmaceutica Sinica B

www.elsevier.com/locate/apsb
www.sciencedirect.com

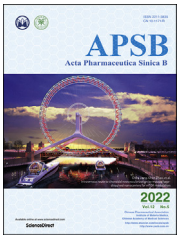

ORIGINAL ARTICLE

Celastrol induces ferroptosis in activated HSCs to ameliorate hepatic fibrosis *via* targeting peroxiredoxins and HO-1

Piao Luo[a,b,†], Dandan Liu[a,†], Qian Zhang[a,†], Fan Yang[c,d,†], Yin-Kwan Wong[a], Fei Xia[a], Junzhe Zhang[a], Jiayun Chen[a], Ya Tian[a], Chuanbin Yang[c], Lingyun Dai[c,*], Han-Ming Shen[e,*], Jigang Wang[a,b,c,d,f,*]

[a]*Artemisinin Research Center, Institute of Chinese Materia Medica, China Academy of Chinese Medical Sciences, Beijing 100700, China*
[b]*Central People's Hospital of Zhanjiang, Zhanjiang 524037, China*
[c]*Department of Urology, the Second Clinical Medical College, Jinan University (Shenzhen People's Hospital), Shenzhen 518020, China*
[d]*Integrated Chinese and Western Medicine Postdoctoral Research Station, Jinan University, Guangzhou 510632, China*
[e]*Faculty of Health Sciences, University of Macau, Taipa, Macau 999078, China*
[f]*Guangdong Provincial Key Laboratory of New Drug Screening, School of Pharmaceutical Sciences, Southern Medical University, Guangzhou 510515, China*

Received 3 September 2021; received in revised form 28 October 2021; accepted 10 November 2021

KEY WORDS

Celastrol;
Ferroptosis;

Abstract Ferroptosis is a form of regulated cell death, characterized by excessive membrane lipid peroxidation in an iron- and ROS-dependent manner. Celastrol, a natural bioactive triterpenoid extracted from *Tripterygium wilfordii*, shows effective anti-fibrotic and anti-inflammatory activities in multiple hepatic diseases. However, the exact molecular mechanisms of action and the direct protein targets of

Abbreviations: α-SMA, alpha smooth muscle actin; ABPP, activity-based protein profiling; ALP, alkaline phosphatase; ALT, alanine aminotransferase; AST, aspartate aminotransferase; CCl_4, carbon tetrachloride; Cel-P, celastrol-probe; CETSA, cellular thermal shift assay; COL1A1, collagen type I alpha-1; COX-2, cyclooxygenase 2; ECM, extracellular matrix; GPX4, glutathione peroxidase 4; HCC, hepatocellular carcinoma; HMGB1, high mobility group protein B1; HO-1, heme oxygenase 1; HSCs, hepatic stellate cells; LPO, lipid peroxidation; PPARγ, peroxisome proliferators-activated receptor γ; PRDXs, peroxiredoxins; ROS, reactive oxygen species; VDACs, voltage-dependent anion channels; VIM, vimentin.

*Corresponding authors. Tel./fax: +86 10 64096302 (Jigang Wang); +86 20 88224987 (Han-Ming Shen); +86 20 22942040 (Lingyun Dai).
E-mail addresses: jgwang@icmm.ac.cn (Jigang Wang), phsshm@nus.edu.sg (Han-Ming Shen), dai.lingyun@szhospital.com (Lingyun Dai).
[†]These authors made equal contributions to this work.

Peer review under responsibility of Chinese Pharmaceutical Association and Institute of Materia Medica, Chinese Academy of Medical Sciences.

https://doi.org/10.1016/j.apsb.2021.12.007

Peroxiredoxin;
HO-1;
Hepatic fibrosis;
ABPP;
Anti-oxidant;
Reactive oxygen species

celastrol in the treatment of liver fibrosis remain largely elusive. Here, we discover that celastrol exerts anti-fibrotic effects *via* promoting the production of reactive oxygen species (ROS) and inducing ferroptosis in activated hepatic stellate cells (HSCs). By using activity-based protein profiling (ABPP) in combination with bio-orthogonal click chemistry reaction and cellular thermal shift assay (CETSA), we show that celastrol directly binds to peroxiredoxins (PRDXs), including PRDX1, PRDX2, PRDX4 and PRDX6, through the active cysteine sites, and inhibits their anti-oxidant activities. Celastrol also targets to heme oxygenase 1 (HO-1) and upregulates its expression in activated-HSCs. Knockdown of PRDX1, PRDX2, PRDX4, PRDX6 or HO-1 in HSCs, to varying extent, elevated cellular ROS levels and induced ferroptosis. Taken together, our findings reveal the direct protein targets and molecular mechanisms *via* which celastrol ameliorates hepatic fibrosis, thus supporting the further development of celastrol as a promising therapeutic agent for liver fibrosis.

1. Introduction

Hepatic fibrosis is among the leading causes of mortality and morbidity worldwide, but unfortunately still lacks effective drugs[1−3]. While the underlying molecular mechanisms of hepatic fibrosis are complicated, it is a dynamic process characterized by extracellular matrix (ECM) deposition, mainly caused by hepatic viral infection, metabolic disorder, alcoholic liver disease and cholestasis[4]. Activation of hepatic stellate cells (HSCs) promotes the secretion of ECM, pro-inflammatory cytokines and proteases to further induce cellular injury and fibrogenesis[5]. Activated-HSCs are now merged as a key driver of human fibrotic liver disease and experimental injury, involved at multiple stages, including acute and chronic hepatitis as well as cirrhosis[6]. Therefore, scavenging activated-HSCs is considered as a promising therapeutic strategy for hepatic fibrosis. Previous studies showed that inducing activated-HSCs to apoptosis, necroptosis or senescence can ameliorate the pathological development of hepatic fibrosis[7,8].

Ferroptosis, a regulated program of cell death, results from the mis-controlled accumulation of membrane lipid peroxidation (LPO) in an iron-dependent manner[9], which is distinguished from other programmed cell deaths such as apoptosis, necrosis or pyroptosis[10]. Factors including the depletion of glutathione (GSH), and the inhibition of cystine/glutamate antiporter system xc^- or glutathione peroxidase 4 (GPX4) can trigger ferroptosis. On the other hand, ferroptosis can be inhibited by iron chelators (*e.g.*, deferoxamine), and lipophilic anti-oxidants (*e.g.*, *N*-acetyl-L-cysteine, ferrostatin-1, and vitamin E)[11,12]. Notably, ferroptosis is closely related to the development and control of various liver diseases, such as steatohepatitis, fibrosis and hepatocellular carcinoma (HCC)[13−17]. Triggering ferroptosis of activated-HSCs is emerging as a novel and promising therapeutic approach for hepatic fibrosis[16,18].

Natural product is a valuable resource for the development of therapeutic agents for many complex diseases including liver fibrosis. We previously demonstrated that artesunate induces ferroptosis in HCC together with sorafenib[19]. Artesunate could also promote ferroptosis of activated-HSCs[20]. In addition, natural products such as chrysophanol and magnesium isoglycyrrhizinate, have been reported to suppress the activation of HSCs and attenuate liver fibrosis *via* regulating ferroptosis[21,22].

Celastrol, a pentacyclic triterpene compound (the chemical structure shown in Fig. 1A), is one of the major bioactive constituents of *Tripterygium wilfordii* Hook F. (TwHF, "Thunder God vine") and has multiple biological properties including anti-tumor, anti-oxidant, anti-obesity, neuroprotective and immunosuppressive effects[23−25]. As early as in 2007, celastrol, along with triptolide, artemisinin, curcumin, and capsaicin, has been suggested as a candidate compound with exceptional potential of becoming a therapeutic agent[26]. Previous works have revealed that celastrol could protect against liver diseases such as acute or chronic hepatitis, fibrosis, cholestatic injury and HCC within the safe dose range[27−31]. To date, celastrol is mostly reported to exert hepatoprotective activities through its anti-oxidant and anti-inflammatory properties. However, the exact molecular mechanism of action of celastrol remains largely elusive.

In this study, we show that celastrol effectively ameliorates carbon tetrachloride (CCl_4)-induced liver injury and hepatic fibrosis *via* promoting ROS-mediated signaling pathways and ferroptosis in activated-HSCs. Celastrol directly binds to peroxiredoxin (PRDX) family members including PRDX1, PRDX2, PRDX4 and PRDX6 (but not PRDX3 and PRDX5), and inhibits their anti-oxidant activities. Moreover, celastrol directly targets heme oxygenase 1 (HO-1) and upregulates its expression level in activated-HSCs. Silencing of PRDXs or HO-1 in HSCs promotes the accumulation of LPO and Fe^{2+}/Fe^{3+}, two key markers of ferroptosis. Collectively, this study reveals that celastrol can directly bind to PRDXs and HO-1 and inhibit their enzymatic activities, resulting in the ferroptosis of activated-HSCs to attenuate hepatic fibrosis.

2. Materials and methods

2.1. Reagents

Celastrol (purity ≥98%) was purchased from Bethealth People Biomedical Technology (Beijing, China). Cell Counting Kit-8 (CCK-8) was purchased from Dojindo (Japan). *N*-Acetyl-L-cysteine and deferoxamine mesylate were obtained from AbMole BioScience (USA). Click chemistry reaction and LC−MS/MS reagents include: TAMRA-azide, Biotin-azide and THPTA (ClickChemistryTools, USA); NaVc and $CuSO_4$ (Sigma−Aldrich, USA); high capacity neutravidin agarose beads, TEAB and sequencing grade modified trypsin (Thermo, USA); Oasis HLB Extraction Cartridge (Waters, USA); Pierce™ Quantitative Fluorometric Peptide Assay Kit (Thermo, USA).

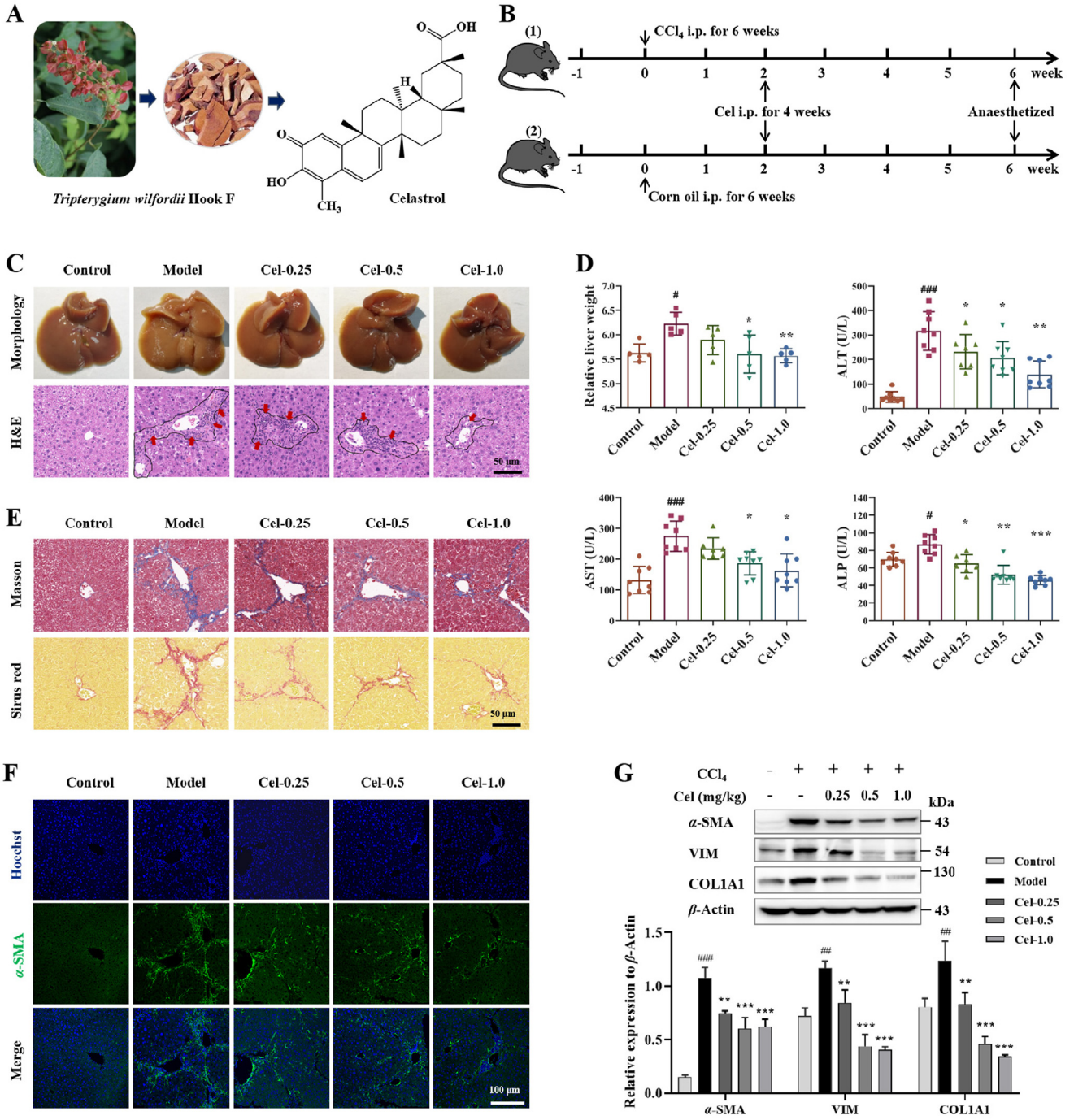

Figure 1 Celastrol ameliorates liver injury and fibrosis. (A) *Tripterygium wilfordii* plant and chemical structure of celastrol (Cel). (B) The scheme of animal experiment. The grouping was as follows: Control; Model (CCl_4, without Cel treatment); Cel-0.25 (CCl_4, 0.25 mg/kg Cel); Cel-0.5 (CCl_4, 0.5 mg/kg Cel); Cel-1.0 (CCl_4, 1 mg/kg Cel). (C) Representative photographs of liver and its H&E staining (scale bar = 50 μm). (D) The percentage ratios of liver/body weight (mean ± SEM, $n = 5$) and the effects of Cel on the levels of serum ALT, AST and ALP in mice (mean ± SEM, $n = 8$; $^{\#}P < 0.05$, $^{\#\#\#}P < 0.001$ *vs*. Control; $^{*}P < 0.05$, $^{**}P < 0.01$, $^{***}P < 0.001$ *vs*. Model). (E) Liver sections with Masson and Sirius Red staining (Scale bar = 50 μm). (F) Immunofluorescence staining of α-SMA (green) in liver tissues (Scale bar = 100 μm). (G) Immunoblotting assay of the levels of α-SMA, VIM and COL1A1 proteins *in vivo* (mean ± SEM, $n = 3$; $^{\#\#}P < 0.01$, $^{\#\#\#}P < 0.001$ *vs*. Control; $^{**}P < 0.01$, $^{***}P < 0.001$ *vs*. Model). *P* values are calculated by one-way ANOVA followed by the Tukey's test.

Specific primary antibodies anti-PRDX1, anti-PRDX2, anti-PRDX3, anti-PRDX4, anti-PRDX5, anti-PRDX6, anti-HO-1 (Abcam, UK), anti-Vimentin, anti-PPARγ, anti-COL1Al (Proteintech, China) and anti-β-actin (Affinity Biosciences, China) were used.

2.2. *Cell culture*

Human hepatic stellate cell (LX-2) and mouse hepatic stellate cell (mHSC) were purchased from the Chinese Academy of Medical Sciences (Beijing, China). These cells were cultured in Dulbecco's

modified Eagle's medium (Corning, New York, USA) with 10% fetal bovine serum (Corning, New York, USA) as well as 100 U/mL penicillin and streptomycin (ThermoFisher, USA), and maintained at 37 °C with 5% CO_2 humidified atmosphere. Cells were passaged regularly and grown to 80%−90% confluence before treatments.

2.3. Detection of cell viability

Cells were seeded in 96-well plate at a density of 5×10^3 cells/well for overnight, and then incubated with different concentrations of celastrol or celastrol-probe (Cel-P) for 12 or 24 h. CCK-8 kit was used to measure the viability of treated cells according to the manufacturer's instructions.

2.4. Animal experiments

All animal experimental procedures were approved by the China Animal Care and Use Committee and the Care and Use of Laboratory Animals of China Academy of Chinese Medical Sciences (Beijing, China). C57BL/6 male mice (22 ± 3 g; Vital River Laboratory Animal Technology, Beijing, China) were maintained under standard conditions. The mice were adapted for 7 days before use. A total of 40 mice were randomly divided into 5 groups, 8 mice per group. They were given corn oil (vehicle, control), CCl_4 (model), CCl_4 + 0.25 mg/kg celastrol, CCl_4 + 0.5 mg/kg celastrol and CCl_4 + 1 mg/kg celastrol, respectively. For CCl_4 model, mice were injected intraperitoneally with CCl_4 diluted 1:3 in corn oil at a dose of 0.5 mL/kg twice a week for 6 weeks[32]. Celastrol was dissolved in corn oil, and injected intraperitoneally to mice once a day for 3 weeks. Blood and liver samples were collected after anaesthetization. A portion of liver was fixed in 4% paraformaldehyde, the rest was flash frozen in liquid N_2.

2.5. Biochemical and histological assays

The levels of aspartate aminotransferase (AST), alanine aminotransferase (ALT) and alkaline phosphatase (ALP) were measured using a biochemistry analyzer (TOSHIBA TBA-40FR, Japan). Liver tissue samples were embedded in paraffin and sectioned. Hematoxylin−eosin (H&E), Masson's trichrome and Sirius Red staining were performed for the examination of histological changes and degree of fibrosis. Hydroxyproline levels in mice livers were quantified using a detection kit (Jiancheng Biotechnology, Nanjing, China) following manufacturer's instructions.

2.6. Western blotting

Proteins were extracted with RIPA buffer supplemented with 1 × protease inhibitor cocktail and separated on SDS-PAGE gel, followed by electro-transferring to PVDF membranes. Next, samples were incubated with the corresponding primary antibodies (listed in Section 2.1.) and secondary antibody. The protein band was visualized using enzyme-linked chemiluminescence reagent in the Enhanced Chemiluminescence Plus detection system (Azure Sapphire RGBNIR, USA). The protein amount was semi-quantified by Image J, and normalized to its corresponding control.

2.7. Cellular imaging

The fluorescence imaging experiments were carried out as previously described[33]. LX-2 cells were grown in 4-chamber glass bottom dishes and treated with 0.5 mL of complete culture medium with Cel-P at various concentrations in the absence or presence of corresponding competitors. After 4 h, cells were washed and fixed with 4% paraformaldehyde at room temperature (RT) for 12 min, and then permeabilized in 0.2% Triton X-100. Cells were subjected to a freshly prepared clicked reaction cocktail (1 mmol/L NaVc, 100 μmol/L THPTA, 1 mmol/L $CuSO_4$ and 50 μmol/L TAMRA-N_3) with gentle shaking for 2 h at RT. Cells were gently washed twice with PBS and once with 0.1% Tween-20 in PBS.

For co-localization studies, cells were fixed and permeabilized as mentioned above, followed by blocking with 5% BSA. Samples were further incubated with different primary antibodies (1:200) at 4 °C overnight. Cells were gently washed twice with 0.1% Tween-20 in PBS, and then incubated with secondary fluorescent antibody (Alexa Fluor 488 or 647, Abcam, UK) (1:500) for 1 h, and then washed again.

Liver tissue sections were treated by a series of dewaxing and dehydrations, and then punched in 0.2% Triton X-100. The remaining procedures were the same as the cell samples.

Eventually, samples were incubated with Hoechst (1:500 dilution) for 30 min at RT prior to acquiring image. All images were acquired with Leica TCS SP8 SR confocal fluorescence microscopy.

2.8. Lipid peroxidation assessment and antioxidant measurement

LPO assay kit (A106-1-2), glutathione assay kit (A006-2-1), Fe^{2+}/Fe^{3+} iron assay kit (A039-2-1), and the fluorescent probe CM-H2DCFDA (E004-1-1) were purchased from Jiancheng Bioengineering Institute (Nanjing, China). H_2O_2 was measured with a Hydrogen Peroxide kit (Beyotime, Shanghai, China). The level of glutathione peroxidase 4 (Anti-GPX4, Abcam, UK) was quantified by immunofluorescence staining.

2.9. In situ and in vitro fluorescence labeling experiments

For fluorescence labeling experiments in live cells[33,34], cells were seeded in 6-well plates until 80%−85% confluence. Cel-P (0.25−4 μmol/L) or DMSO was added for 3 h, followed by medium removal and cell washing twice with pre-chilled PBS. RIPA buffer with protease inhibitor cocktail was used for protein extraction. The soluble protein was obtained by centrifugation and the concentration was measured by BCA kit. Equal amounts of lysate proteins (200 μg) from different groups were taken and incubated with the click chemistry reaction cocktail (1 mmol/L NaVc, 100 μmol/L THPTA, 1 mmol/L $CuSO_4$ and 50 μmol/L TAMRA-azide). The reaction was incubated with vigorous shaking at RT for 2 h. Labeled protein was precipitated by pre-chilled acetone (−20 °C). Samples were dissolved in 40 μL 1 × loading buffer, before being loaded on SDS-PAGE gel and separated by electrophoresis, and then visualized by fluorescence scanning in laser scanner (Azure Sapphire RGBNIR, USA). Finally, the SDS-PAGE gel was stained with Instant Blue Coomassie Protein Stain.

For fluorescence labeling of recombinant protein, proteins (0.5−1 μg/μL) in PBS buffer were incubated with probe for 1 h at RT with gentle shaking, and then clicked with pre-mixed click cocktail. Samples were then separated on SDS-PAGE and visualized as described above. For competitive labeling experiments, samples were pre-treated with competitors for 30−120 min and then processed as mentioned above.

2.10. Pull down and LC−MS/MS based targets identification

Experimental procedures were similar to what was previously described[33]. LX-2 cells were pre-treated with competitors for 1 h, followed by adding the Cel-P (2 μmol/L) or DMSO in fresh medium. After incubation for 4 h, the soluble proteins were extracted to perform click reaction as described above. The air-dried samples were dissolved in 1.5% SDS in PBS. Then the final concentration of SDS was diluted to 0.1% with PBS and centrifuged at RT for 10 min. The sample solution was incubated with 50 μL streptavidin beads for 4 h at RT, and beads were washed with 5 mL PBS containing 1% SDS (thrice) and 0.1% SDS (once), and 6 mol/L urea (thrice) and PBS (twice).

For targets identification by LC−MS/MS, the enriched proteins from streptavidin beads were separated by SDS-PAGE followed by Coomassie staining. The band corresponding to the specific molecular weight region (20−55 kDa) were excised, cut to small pieces, and then washed with 25 mmol/L ammonium bicarbonate buffer and 50% acetonitrile in 25 mmol/L ABB buffer. After dehydration in Speedvac, the samples were reduced by dithiothreitol (DTT) and alkylated by iodoacetamide (IAA). Then the samples were incubated with trypsin to digested into peptides overnight at 37 °C. Peptide solution was desalted on C18 column. TMT10 plex Mass Tag Labeling reagents (Thermo) were used for peptide labeling according to the instructions. Finally, samples were analyzed by LC−MS/MS (Thermo).

For pull down-Western blot analysis, the bound proteins were detected by Western blot assay with the same procedures mentioned above.

2.11. Target protein analysis and gene ontology (GO) enrichment

According to the TMT signals of DMSO (control) group, Cel + Cel-P (compete) and Cel-P (treatment) group, the *P* values (Cel-P/DMSO and Cel-P/Compete) were generated by using 1 sample *t*-test as previously described[35]. The target proteins were selected based on the absolute fold change >1.2 and *P* value < 0.05. GO enrichment analysis were performed on the selected proteins using the "clusterprofiler" package (version 3.18.1) in R[36].

2.12. Cellular thermal shift assay (CETSA)−Western blot (WB)

CETSA−WB experiment was carried out as previously described[37,38]. Briefly, the soluble protein lysate of LX-2 cells was aliquoted into PCR tubes and treated with celastrol (20 μmol/L) or DMSO for 1 h at RT prior to CETSA heat pulse. The solutions were heated at the indicated temperatures (37−73 °C) for 3 min, followed by cooling at 4 °C for 3 min in a thermocycler (Applied biosystems, USA). After centrifugation for 20 min (20,000×*g*, 4 °C), the soluble supernatant was subject to Western blotting.

2.13. Expression and purification of recombinant proteins

Human *PRDX1*, *PRDX2*, *PRDX4*, *PRDX6* and *HO-1* genes, as well as the mutants of *PRDX1* and *PRDX2* were subcloned into pET28a vector with a 6 × His-tag fusion (Sangon, Shanghai, China). The *Escherichia coli* BL21 was transformed with the expression plasmid, and cultured in LB medium containing 50 μg/mL kanamycin (200 rpm, 37 °C) to OD_{600} of 0.6−0.8, and the protein expression was induced with 0.4 mmol/L IPTG for 14 h at 16 °C. Bacterial pellet was suspended in lysis buffer (200 mmol/L NaCl, 20 mmol/L Tris−HCl, 1 mmol/L PMSF, 1 × protease inhibitor cocktail, pH 8.0) and disrupted by sonication. After centrifugation (12,000 × *g* for 30 min at 4 °C), supernatant was applied to Ni-NTA beads column (Qiagen, USA) and washed with 30 mL binding buffer (200 mmol/L NaCl, 20 mmol/L Tris−HCl, 20 mmol/L or 50 mmol/L imidazole, pH 8.0). Recombinant proteins were eluted with 200 mmol/L NaCl, 20 mmol/L Tris−HCl and 200 mmol/L imidazole, pH 8.0 buffer. The protein concentration was determined with BCA kit. The purity and integrity of the purified proteins was verified on SDS-PAGE gel by Coomassie brilliant blue.

2.14. UV−visible absorption spectra assay

The UV−visible absorption spectra of celastrol in PBS buffer was measured at 300−600 nm by a multimode 96-well plate reader (PerkinElmer, USA). Celastrol (100 μmol/L) was incubated with or without the indicated proteins (20 μmol/L), and the absorbance spectra was recorded.

2.15. Molecular docking

The crystal structures of proteins were retrieved from Protein Data Bank (PRDX1: 4XCS; PRDX2: 5IJT; PRDX4: 3TKQ; PRDX6: 5B6N; HO-1: 4WD4). Docking process: Discovery Studio Client was used to perform dehydration and hydrogenation of proteins. Pyrx-0.8 and AutoDock Vina[39] were used for molecular docking, and Pymol software for mapping.

2.16. Activity assay of recombinant human PRDX proteins

The peroxidase activities of recombinant human PRDX proteins were measured as described previously[40,41]. The enzymatic activity of PRDX2 was measured by adding 10 μL H_2O_2 (final 50 μmol/L) into different concentrations of rhPRDX2 solutions, followed by assessing the residual H_2O_2 level using Hydrogen Peroxide Assay Kit (Beyotime, Shanghai, China). To measure the inhibition of celastrol on the peroxidase activities PRDXs, rhPRDX proteins (30 μmol/L) were incubated with DMSO or celastrol (5 μmol/L) for 20 min at room temperature, followed by measurement as described above.

2.17. HO-1 activity assay

The HO-1 activity assay was carried out as previously described[42]. Briefly, 99 μL of 5 μmol/L rhHO-1 and 50 μmol/L hemin solution in 100 mmol/L MOPS pH 7.0 was incubated with 1 μL DMSO or celastrol (5−20 μmol/L final concentration) for 20 min at RT. And then 100 μL of 2 mmol/L L-ascorbic acid and 400 μmol/L Ferene-S mixed reagent was added. The absorbance of Ferene-S and biliverdin was determined using Spark 10M plate reader (Tecan, Switzerland) at 593 and 670 nm, respectively.

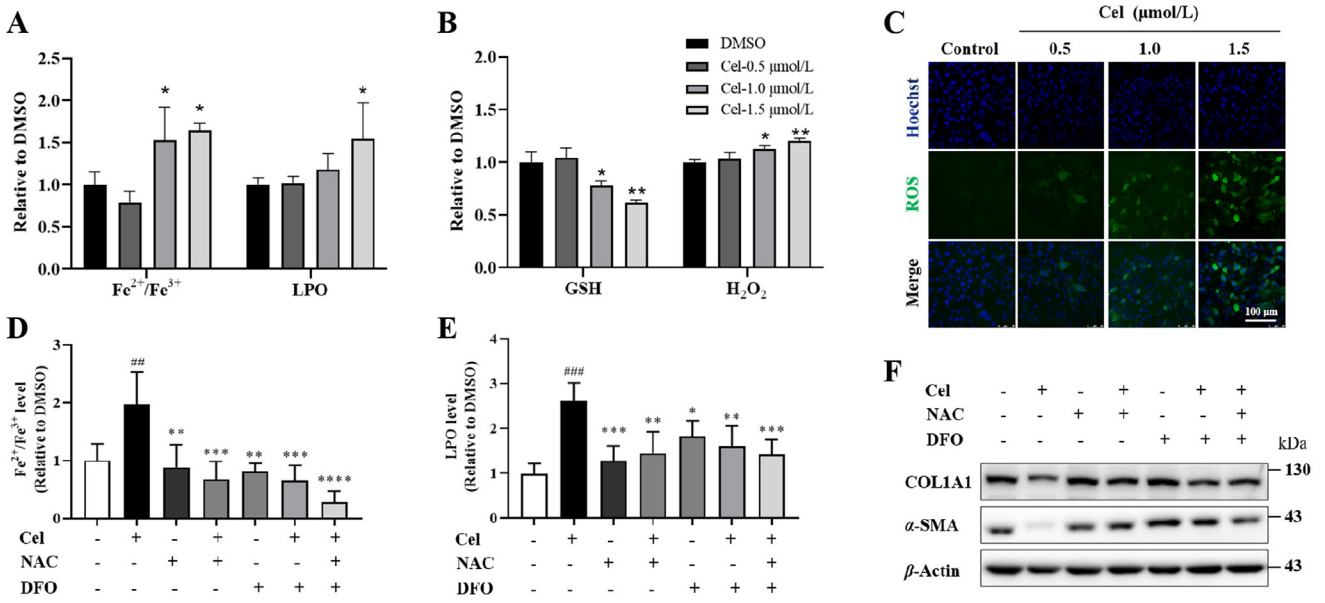

Figure 2 Celastrol exerts anti-fibrosis effect by inducing ferroptosis in activated-HSCs. (A) Levels of Fe^{2+}/Fe^{3+} and LPO after celastrol treatment in human hepatic stellate LX-2 cells (mean ± SEM, $n = 3$; $^{*}P < 0.05$, $^{**}P < 0.01$ *vs*. DMSO). (B) Levels of GSH and H_2O_2 after celastrol treatment in LX-2 cells (mean ± SEM, $n = 3$; $^{*}P < 0.05$, $^{**}P < 0.01$ *vs*. DMSO). (C) Immunofluorescence staining of intracellular ROS (green) in LX-2 cells (scale bar = 100 μm). (D, E) The effect of DFO and/or NAC on celastrol-induced ferroptosis (as indicated by two ferroptosis-associated markers: Fe^{2+}/Fe^{3+} and LPO level) in LX-2 cells (mean ± SEM, $n = 3$; $^{\#\#}P < 0.01$, $^{\#\#\#}P < 0.001$ *vs*. DMSO; $^{*}P < 0.05$, $^{**}P < 0.01$, $^{***}P < 0.001$, $^{****}P < 0.0001$ *vs*. Cel). (F) The effect of DFO and/or NAC on the anti-fibrosis effect of celastrol, as indicated by the immunoblotting of COL1A1 and α-SMA protein levels, in LX-2 cells. *P* values are calculated by one-way ANOVA followed by the Tukey's test.

2.18. *RNA interference and transfection*

Complementary oligonucleotides sequences of siRNAs (Supporting Information Table S1) were designed and synthesized by Sangon (Shanghai, China). These siRNA or negative control (NC) vectors were transfected into LX-2 cells by lipofectamine 2000.

2.19. *Statistical analysis*

All data are presented as mean ± standard error of mean (SEM) for 3 independent experiments. Statistical analysis was carried out by one-way ANOVA followed by the Tukey's test in multiple groups. Unpaired two-tailed *t* test was performed in two groups. Statistical analysis was performed in GraphPad Prism 8.0 software (San Diego, CA, USA).

3. Results

3.1. *Celastrol ameliorates CCl_4-induced hepatic injury and fibrosis in mice*

We first set out to evaluate the pharmacological activities of celastrol on carbon tetrachloride (CCl_4)-induced liver damage and fibrosis *in vivo*. The animal experiment was designed and carried out as depicted in Fig. 1B. Celastrol remarkably ameliorated CCl_4-induced liver damage and morphological changes, as evidenced by reduced hemorrhagic necrosis and inflammatory cell infiltration (Fig. 1C). Compared to the sole CCl_4-induced model group, celastrol not only normalized the ratio of liver/body weight (Fig. 1D), but also markedly reduced the serum levels of AST, ALT and ALP, the three key diagnostic markers used in liver function test, indicating the normalization of liver functions (Fig. 1D). Moreover, celastrol significantly reduced the deposition of collagen fibers as indicated by Masson and Sirius Red staining (Fig. 1E, Supporting Information Fig. S1A and S1B). Hydroxyproline examination further supported that the increase of collagen production was abrogated upon celastrol treatment (Fig. S1C). Celastrol inhibited the expressions of alpha smooth muscle actin (α-SMA, a marker for activated fibrogenic cells), vimentin (VIM, a pro-fibrotic factor and a marker for HSCs activation) and collagen type I alpha-1 (COL1A1) proteins both *in vivo* (Fig. 1F and G) and *in vitro* (Supporting Information Fig. S2A), also upregulated the expression of peroxisome proliferators-activated receptor γ (PPARγ) in human hepatic stellate LX-2 cells (Fig. S2B). These results demonstrate that celastrol ameliorated CCl_4-induced hepatic damage and fibrosis.

3.2. *Celastrol suppresses hepatic fibrosis via promoting ROS signaling and inducing ferroptosis in activated-HSCs*

Currently, there is only a single report that celastrol could ameliorate hepatic fibrosis *via* regulating inflammation[31]. We hypothesized that celastrol could work *via* inducing the ferroptosis of activated-HSCs. Therefore, we first examined the expression level of a key negative regulator of ferroptosis process—glutathione peroxidase 4 (GPX4) upon celastrol treatment in fibrotic mice. GPX4 proteins were accumulated in fibrotic livers, and were mainly co-localized with α-SMA-positive activated HSCs, suggesting the importance of controlling ferroptosis in activated-HSCs (Supporting Information Fig. S3A). Similarly, cyclooxygenase 2 (COX-2), an inducible enzyme responsible for the biosynthesis of prostanoid which is a ferroptosis-sensitive phospholipid, was also elevated in

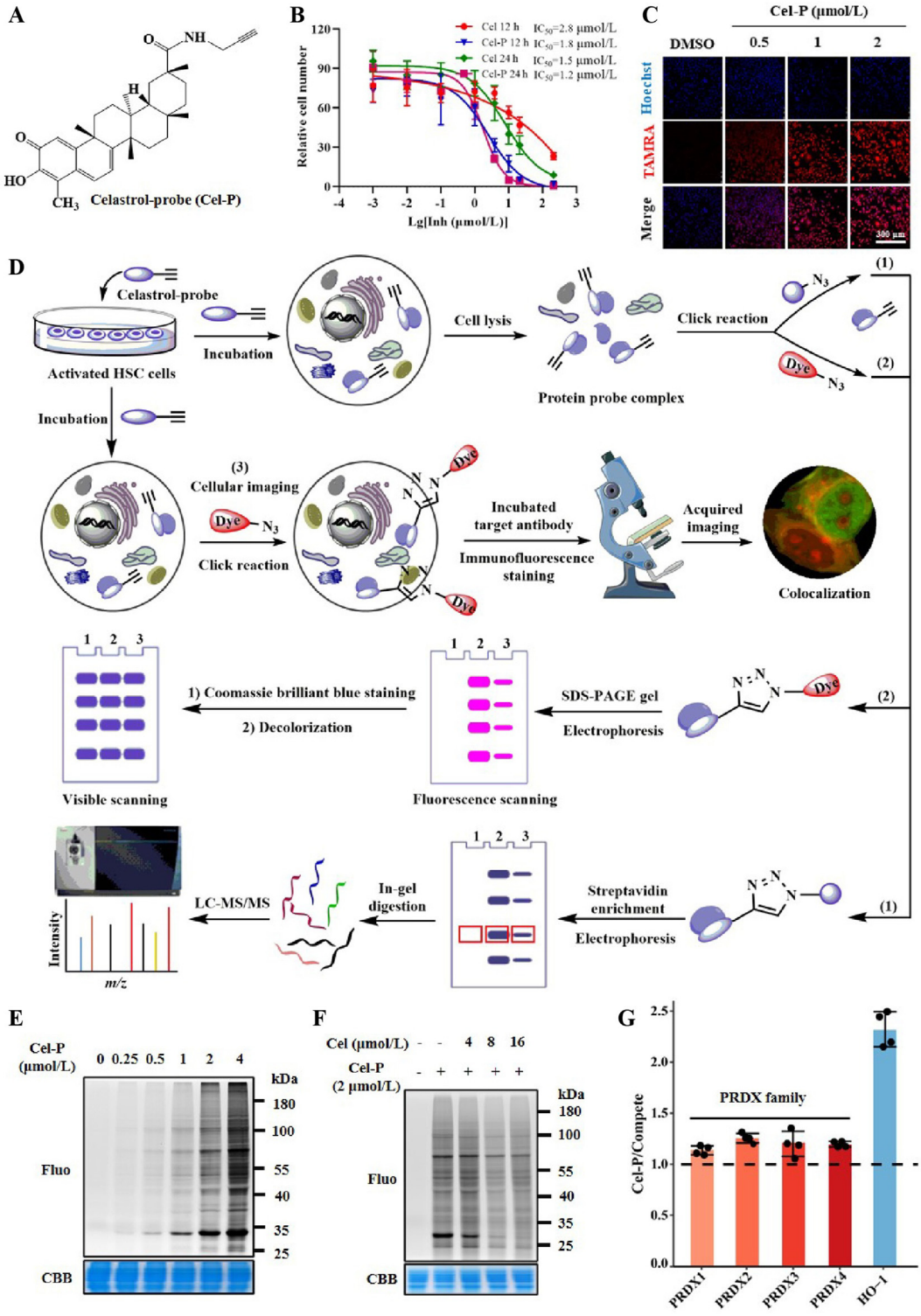

Figure 3 The ABPP in combination with LC−MS/MS approach to profile and identify the targets of celastrol. (A) Chemical structure of celastrol-probe. (B) Inhibition of LX-2 cell proliferation by celastrol (Cel) and celastrol-probe (Cel-P) in a dose-dependent manner (mean ± SEM, $n = 3$). (C) Immunofluorescence staining of the distribution of Cel-P in LX-2 cells (scale bar = 200 μm). (D) Overall workflow for ABPP profiling of potential celastrol targets. (E) *In situ* protein labelling with Cel-P in a dose-dependent manner in LX-2 cells. (F) The competition of *in situ* protein labeling with Cel-P by Cel in LX-2 cells. (G) Bar plot showing the differential enrichment of a few representative target proteins in Cel-P *vs*. "Compete" (Cel-P + 4 × Cel) group, each point represents one calculated ratio value of Cel-P/Compete (mean ± SD, $n = 4$).

activated-HSCs (Fig. S3B). Interestingly, GPX4 level was downregulated in a dose-dependent manner after treatment of celastrol (Fig. S3A).

We measured the levels of two ferroptosis markers (iron ion Fe^{2+}/Fe^{3+}, and LPO) and several markers for cellular oxidative stress [glutathione (GSH), H_2O_2, and reactive oxygen species (ROS)] in LX-2 cells. Interestingly, celastrol induced the accumulation of Fe^{2+}/Fe^{3+} and LPO (Fig. 2A). Moreover, celastrol downregulated the level of anti-oxidant GSH and upregulated the level of oxidative H_2O_2 and ROS in LX-2 cells (Fig. 2B, C and Fig. S3C). We also evaluated the effects of celastrol on three main cell types in livers (hepatocytes, macrophages, as well as HSCs). The results suggest that celastrol is able to modulate the expression levels of GPX4 and COX-2 in different cells—only in HSCs, GPX was downregulated and COX-2 was upregulated, indicating the induction of ferroptosis (Fig. S3D−S3F). In addition, LX-2 showed higher sensitivity and lower tolerance to celastrol in comparison with hepatocytes and macrophages (Fig. S3G). Taken together, these observations indicate that celastrol promoted ferroptosis of activated-HSCs *in vitro* and *in vivo*.

3.3. *Inhibiting ferroptosis abolishes the anti-fibrosis activity of celastrol*

To confirm the involvement of ferroptosis in the anti-fibrosis activity of celastrol, we determined whether inhibiting ferroptosis abolishes the anti-fibrosis effect of celastrol. Two ferroptosis inhibitors deferoxamine (DFO, an iron chelator) and *N*-acetyl-L-cysteine (NAC, a cysteine prodrug serving as a lipophilic antioxidant) were used. LX-2 cells were incubated with celastrol, and co-treated with DFO and/or NAC for 24 h. As expected, LX-2 cells treated with celastrol showed more LPO, and higher level of Fe^{2+}/Fe^{3+}, indicating the development of ferroptosis, whereas co-treatment with DFO and/or NAC can alleviate the loss of cell viability, reduce the levels of LPO, Fe^{2+}/Fe^{3+} and ROS, and increase the GSH level (Fig. 2D and E, and Supporting Information Fig. S4A−S4C). Moreover, Western blotting results show that co-treatment of DFO and/or NAC significantly attenuated the reduction of α-SMA and COL1A1 levels by celastrol (Fig. 2F, Fig. S4D and S4E). Taken together, these findings demonstrate that celastrol ameliorated hepatic fibrosis by regulating ferroptosis and ROS signaling pathway.

3.4. *Celastrol directly targets to peroxiredoxins and HO-1*

To identify the potential target proteins of celastrol, a celastrol-probe (Cel-P) was designed and synthesized with a clickable alkyne tag (Fig. 3A and Supporting Information Scheme S1). Firstly, we examined the anti-fibrosis efficacy of Cel-P in human LX-2 and mouse HSC (mHSC) cells. Cel-P showed similar cellular potency as the unmodified celastrol (Fig. 3B and Supporting Information Fig. S5A). Same as unmodified celastrol, Cel-P also abated the expressions of VIM, and upregulated the expression of PPARγ in LX-2 cells (Fig. S5B and S5C), suggesting that the attached alkyne tag does not affect the activity of celastrol. We utilized the alkyne tag in Cel-P to perform a click chemistry reaction with a red fluorescent dye TAMRA-azide to examine its subcellular localization[34], suggesting that it is largely distributed in cytoplasm and nucleus (Fig. 3C, D, and Fig. S5D). We then performed *in situ* labeling of LX-2 and mHSC cells with Cel-P. Many proteins were labeled by Cel-P in a dose-dependent manner (Fig. 3E). In addition, co-incubation with excess celastrol could compete with the labeling of Cel-P *in situ* in both LX-2 and mHSC cells, as well as in LX-2 cell lysate (Fig. 3F and Fig. S5E−S5H).

Next, the proteins bound to Cel-P were identified by ABPP strategy. LX-2 cells were first incubated with Cel-P with or without the competition of celastrol, and then the proteins extract from the cells was incubated with biotin-alkyne. The celastrol labeled proteins were affinity-purified on streptavidin beads, eluted for electrophoresis on SDS-PAGE gel, and identified by LC−MS/MS. Compared to the "Compete" group, heme oxygenase 1 (HO-1) was significantly higher in the Cel-P group (Fig. 3G and Supporting Information Fig. S6A). Interestingly, we also noticed the relative enrichment of peroxiredoxin (PRDX) family proteins in the Cel-P group (Fig. 3G, Fig. S6A and S6B). PRDX proteins are an important family of nonselenium peroxidases with six members[43,44]. Among them, PRDX6 has been recently reported as a regulator of ferroptosis[45]. This caught our attention and decided to investigate further.

We then performed pull-down experiment to verify the direct interactions between celastrol and the PRDX family members. The results show that Cel-P successfully pulled down PRDX1, PRDX2, PRDX4 and PRDX6, but not PRDX3 and PRDX5, after harsh washing conditions (Fig. 4A). In addition, the binding of Cel-P to these four PRDX proteins could be competed away with unmodified celastrol (Fig. 4A). As expected, Cel-P could also specifically pull-down HO-1 (Fig. 4A). The immunofluorescence staining also supported the co-localization of Cel-P with PRDX1, PRDX2, PRDX4, PRDX6 or HO-1 in LX-2 cells (Fig. 4B and Supporting Information Fig. S7A). In addition, a cell lysate CETSA−WB experiment was carried out to support the direct interaction with celastrol (Fig. 4C). Protein extracts from LX-2 cells were treated with celastrol (20 μmol/L) or DMSO, and subjected to CETSA heat pulse followed by soluble protein extraction and quantification. Interestingly, PRDX1, PRDX2, PRDX4, PRDX6 and HO-1 all displayed significant thermal stabilization in celastrol treatment group (Fig. 4D and Fig. S7B). Collectively, these findings suggest that celastrol may directly bind to PRDX1, PRDX2, PRDX4, PRDX6 and HO-1.

3.5. *Celastrol inhibits the anti-oxidant activities of PRDXs without affecting their expressions*

We then measured the expression levels of PRDX1, PRDX2, PRDX4, PRDX6 and HO-1 proteins after celastrol treatment in LX-2 cells or in CCl_4-induced fibrotic mice. The results show that celastrol hardly affected the expressions of PRDX1, PRDX2, PRDX4 and PRDX6 (Fig. 5A and B). As for HO-1 protein, although not showing statistical significance, higher doses of celastrol tend to upregulate the HO-1 level *in vivo* (Supporting Information Fig. S8A). The *in vitro* results on LX-2 cells supported the significant upregulation of the HO-1 level by celastrol (Fig. S8B). We further explored whether celastrol inhibits the anti-oxidant activity of recombinant human PRDXs (rhPRDX1, rhPRDX2, rhPRDX4 and rhPRDX6), by a H_2O_2 reduction assay. The results show that celastrol could significantly suppress the peroxidase activity of rhPRDXs for H_2O_2 reduction (Fig. 5C, Supporting Information Fig. S9A). We also explored whether celastrol inhibits the enzymatic activity of HO-1. HO-1 catalyzes the degradation of free heme

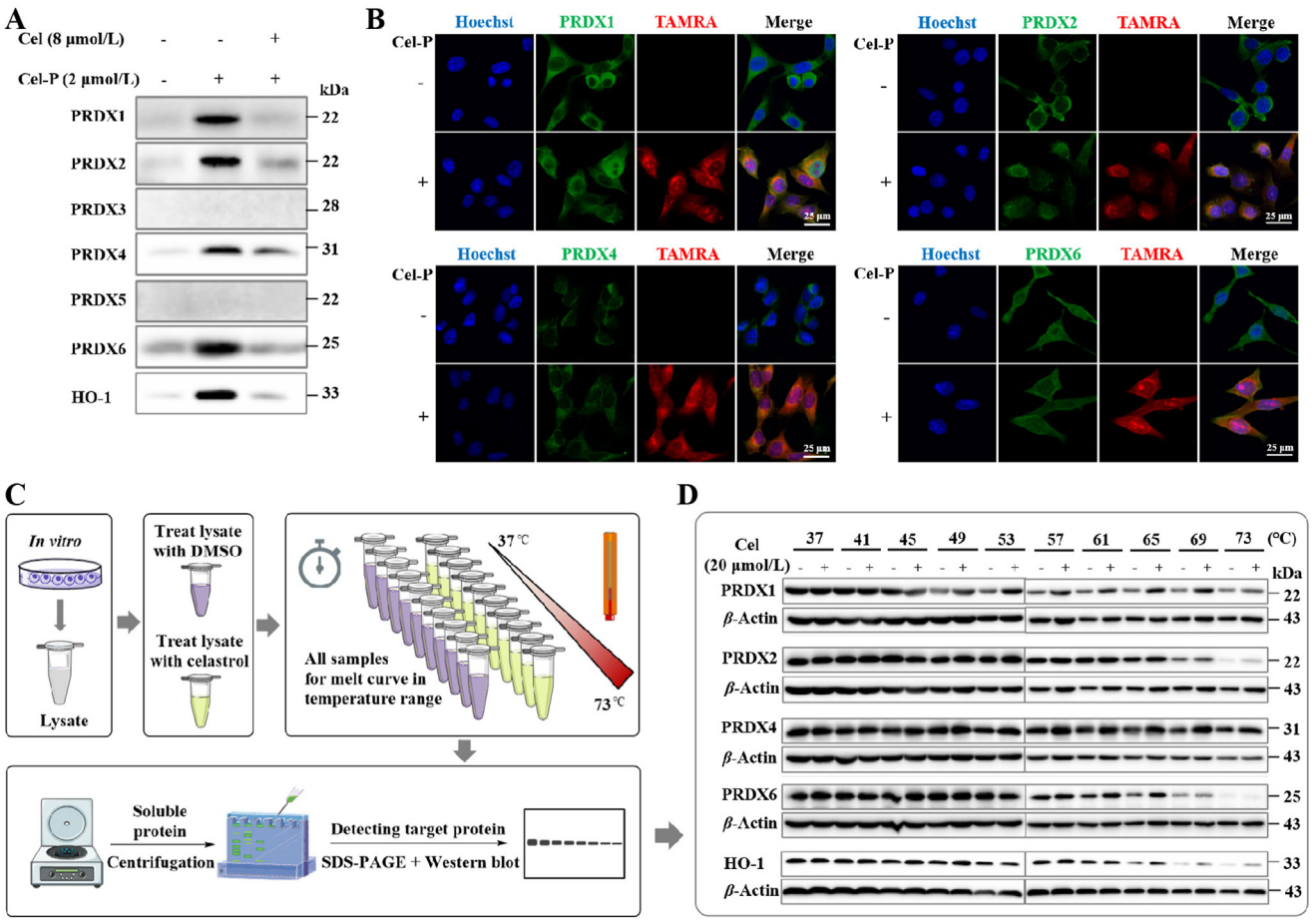

Figure 4 Celastrol directly binds to PRDX and HO-1 proteins. (A) Pull-down followed by immunoblotting to verify celastrol directly targeting to PRDX or HO-1 proteins *in situ*. (B) Immunofluorescence staining of PRDX proteins (green) and Cel-P clicked with a red fluorescence dye TAMRA (scale bar = 25 μm). (C) Scheme of CETSA−WB experiment. (D) CETSA−WB experiment to further confirm the interaction between celastrol and PRDX or HO-1 proteins.

into CO, Fe^{2+} and biliverdin, so we measured the production of Fe^{2+} and biliverdin by rhHO-1 with or without celastrol. The results suggest that celastrol can affect the catalytic activity of HO-1 only at a high concentration of 20 μmol/L (Fig. S9B). In summary, celastrol effectively inhibits the catalytic activities without affecting the expressions of PRDXs. Meanwhile, celastrol upregulates the expression of HO-1, and only partially inhibits the catalytic activity of HO-1 at high concentrations.

3.6. Reactive cysteines of PRDXs are the binding site for celastrol

We further explored how celastrol inhibits the catalytic activities of PRDXs. The recombinant PRDX proteins were incubated with Cel-P, followed by click reaction with TAMRA-azide as a reporter. The labeling was in a dose-dependent manner (Fig. 6A−D), suggesting that celastrol covalently modified PRDX1, PRDX2, PRDX4 and PRDX6. Next, a competition experiment was carried out, in which rhPRDX proteins were first treated with excessive compounds including celastrol (Cel), triptolide (TL) or iodoacetamide (IAA, an active alkylating reagent of cysteine)[46], followed by incubation with Cel-P and click reaction with TAMRA-azide. Interestingly, celastrol and TL competed away Cel-P similarly as IAA, although with slightly lower potency (Fig. 6E−H). Noteworthy, celastrol, TL and IAA also effectively competed away the labeling of rhPRDX proteins by IAA-yne (IAA incorporated with an alkyne moiety), with the only exception of TL for PRDX4 (Fig. 6I−L). Overall, these results indicate that reactive cysteine residues of PRDXs are the binding sites for celastrol.

A UV−visible spectroscopy method has been used for monitoring the formation of covalent adducts between celastrol and nucleophilic thiol[47]. The absorption spectrum of celastrol shows a maximal peak at 450 nm in a dose-dependent manner (Fig. 7A). The reduction of the spectrum peak indicates that the reduction of free celastrol presumably due to the formation of covalent adducts. We successfully exploited this property to confirm the reactivity of celastrol with PRDX1, PRDX2, PRDX4 and PRDX6 proteins (Fig. 7B).

To find out the exact binding sites, we first carried out molecular docking analysis on the solved structures of PRDX proteins. The analysis results suggest the interactions between celastrol and Cys83 of PRDX1, Cys172 and Cys51 of PRDX2, Cys124 of PRDX4, as well as Cys91 of PRDX6 (Fig. S10A−S10D). Next, we conducted site-directed mutagenesis on the four cysteines of PRDX1 and on the three cysteines of PRDX2 to generate a series of cysteine-mutated variants. These recombinant PRDX1 and PRDX2 mutant proteins were subjected to Cel-P labeling and click reaction with TAMRA-azide dye (Fig. 7C and D). This result indicates that celastrol mainly covalently modified Cys83 and Cys173 of PRDX1,

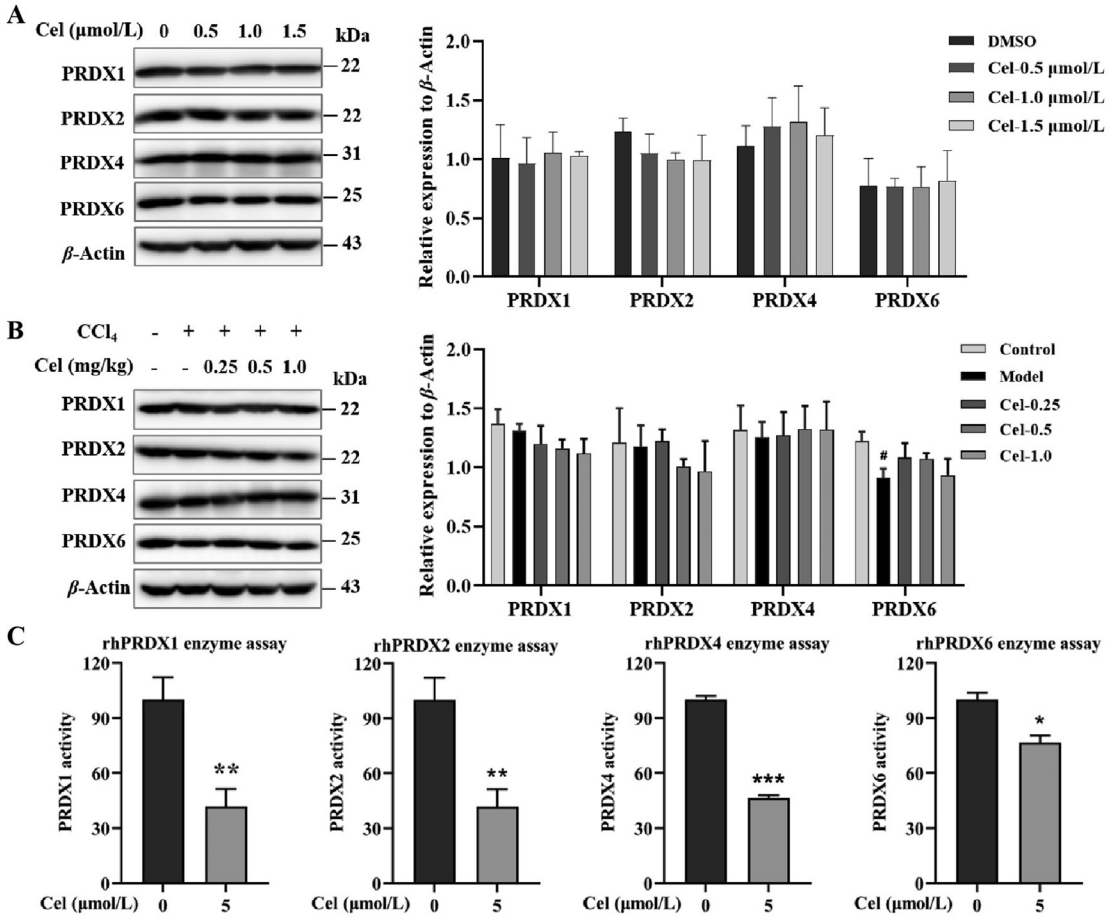

Figure 5 Celastrol inhibits the anti-oxidant activities without affecting expression levels of PRDX proteins. (A) Western blot assay of PRDX1, PRDX2, PRDX4 and PRDX6 in LX-2 cells after treatment with Cel and the corresponding densitometry analysis (mean ± SEM, $n = 3$). (B) Western blot assay of PRDX1, PRDX2, PRDX4 and PRDX6 in CCl_4-induced mice treated with or without celastrol and the corresponding densitometry analysis (mean ± SEM, $n = 3$; $^{\#}P < 0.05$ *vs*. Control). (C) The peroxidase/anti-oxidant activity of rhPRDXs (30 μmol/L) with or without celastrol (5 μmol/L) in H_2O_2 reduction assay (mean ± SEM, $n = 3$; $^{*}P < 0.05$, $^{**}P < 0.01$, $^{***}P < 0.001$ *vs*. Cel 0 μmol/L). *P* values are calculated by unpaired two-tailed *t* test.

but to a much less extent Cys52 and Cys71 (Fig. 7C). Similarly, for PRDX2, the main covalent binding site was Cys172 (Fig. 7D). In both cases, the experimental results largely fit in well with the molecular docking analysis result. Since Cys-SH group of PRDXs is the primary site of oxidation by H_2O_2, the covalent modification of the thiol group by celastrol could be the reason why the anti-oxidant activities of PRDXs are impaired. Interestingly, while HO-1 protein is cysteine-free, the absorption spectrum peak of celastrol was also reduced when in the presence of HO-1 (Fig. S10E). By using docking analysis, we found that C-6 site of celastrol could form a salt bridge with Arg25 of HO-1 (Fig. S10F), which might be the reason of how HO-1 reduces the absorption of celastrol.

3.7. Knockdown of PRDX or HO-1 proteins aggravates ROS signaling and induces ferroptosis

To functionally validate that PRDX and HO-1 proteins are the targeted proteins of celastrol in the induction of ferroptosis to exert its anti-fibrosis function, small interfering RNA (siRNA) for these target proteins were designed and synthesized (Table S1). LX-2 cells were transfected with the corresponding siRNAs for 72 h, followed by Western blotting analysis of the levels of the target proteins (Supporting Information Fig. S11A). The results also show that silencing of *PRDX1*, *PRDX2*, *PRDX4*, *PRDX6* or *HO-1* genes resulted in the accumulation of LPO and Fe^{2+}/Fe^{3+}, albeit at varying extents (Fig. 8A and B). Moreover, knockdown of PRDX or HO-1 proteins decreased the cellular GSH level (Fig. 8C), and increased ROS levels (Fig. 8D, Fig. S11B and S11C). The addition of celastrol to *PRDX*- or *HO-1*-knockdown cells induced significantly more ROS (Fig. 8D, Fig. S11B and S11C). Finally, the *PRDX*- or *HO-1*-knockdown could induce the loss or suppression of HSCs to a certain extent, as indicated by the reduced α-SMA protein level, and more importantly, this could be reversed by either of the two ferroptosis inhibitors DFO and NAC (Fig. S11D). Altogether, these results indicate that knockdown of PRDX proteins or HO-1 induced ferroptosis and aggravate ROS signaling mediated by celastrol (Fig. 9).

4. Discussion

Hepatic fibrosis is one of the main chronic fibroproliferative diseases, and could unconsciously evolve into liver cirrhosis, even hepatocellular carcinoma[48,49]. During the pathological process of liver fibrosis, activated-HSCs play a vital role in ECM

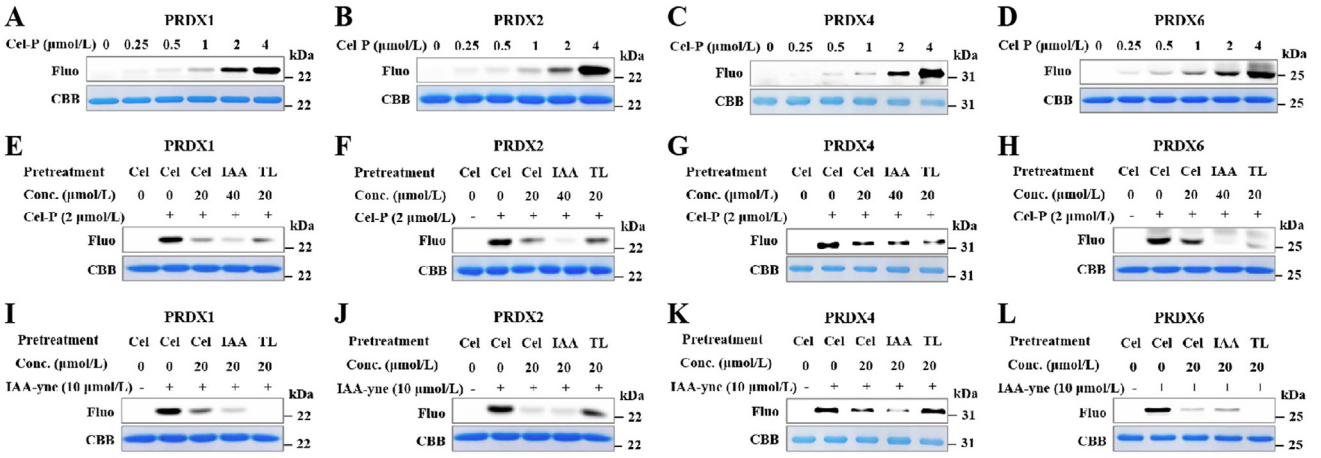

Figure 6 Celastrol binds to the cysteines of PRDX proteins. (A−D) Cel-P labeling of rhPRDX1, rhPRDX2, rhPRDX4 or rhPRDX6 proteins in a dose-dependent manner. (E−H) Cel-P labeling of rhPRDX1, rhPRDX2, rhPRDX4 or rhPRDX6 proteins in the presence or absence of different competitors. (I−L) IAA-yne labeling of rhPRDX1, rhPRDX2, rhPRDX4 or rhPRDX6 proteins in the presence or absence of different competitors (celastrol, Cel; triptolide, TL; or iodoacetamide, IAA).

deposition[50]. Natural products targeting to depress or scavenge activated-HSCs have merged as a revolutionary therapeutic strategy for the treatment of liver fibrosis[20,22,51]. Celastrol is one of the most promising candidate therapeutic molecules from *T. wilfordii* and has attracted widespread attention. Although there was a recent report about the anti-hepatic fibrosis activity of celastrol, possibly through its anti-inflammatory effect *via* activation of AMPK−SIRT3 signaling[31], the exact mechanisms and direct targets of celastrol remain to be explored.

We first show that celastrol triggers ferroptosis of activated-HSCs to inhibit hepatic fibrosis, but how does celastrol regulate ferroptosis or ROS signaling and exert its anti-liver fibrosis effect? To discover the underlying mechanisms and cellular target proteins of celastrol, we designed and synthesized a celastrol-probe with a clickable alkyne tag. Subsequently, with combined usage of the ABPP, bio-orthogonal click chemistry and LC−MS/MS, the target proteins covalently bound to celastrol were identified. Previously, we had utilized the similar approach to deconvolute

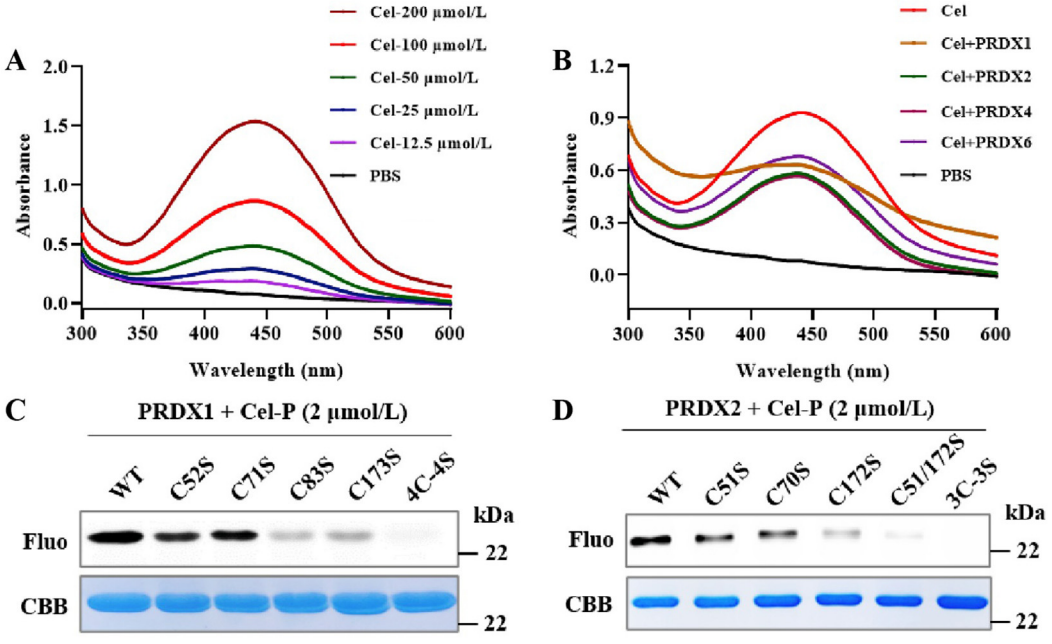

Figure 7 Celastrol binds to PRDXs at reactive cysteine residues and inhibits their activities. (A) Absorption spectra of celastrol at different concentrations (0−200 μmol/L). (B) Absorption spectra of celastrol (100 μmol/L) after incubation with rhPRDX1, rhPRDX2, rhPRDX4 or rhPRDX6 (15 μmol/L). (C, D) Mutation analysis on cysteine sites of PRDX1 and PRDX2 proteins. WT or mutants recombinant PRDX1 (C) and PRDX2 proteins (D) were incubated with Cel-P for 45 min were incubated with Cel-P for 45 min, clicked with a fluorescent dye, followed by SDS-PAGE analysis and fluorescence scanning.

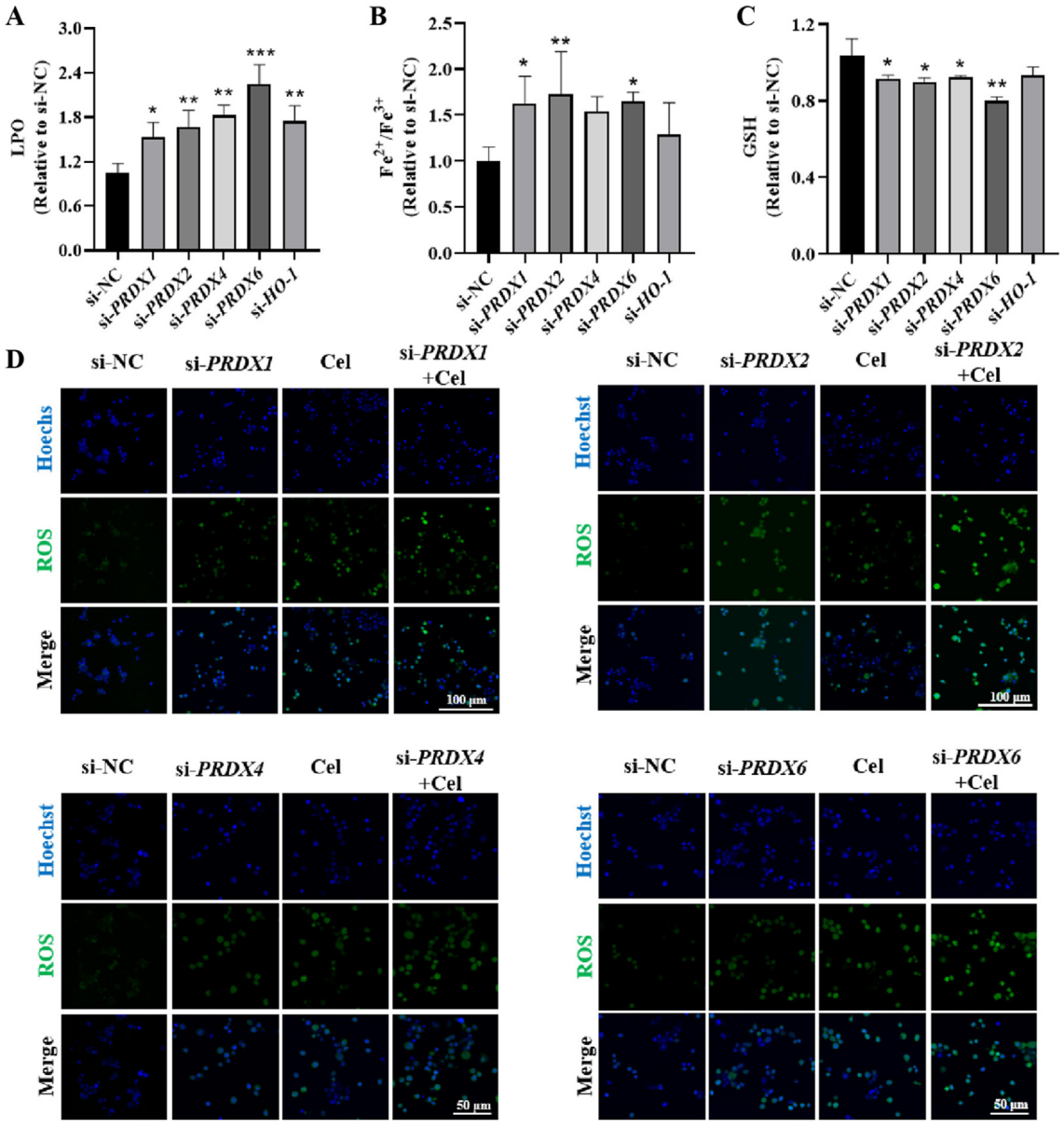

Figure 8 Induction of ROS and ferroptosis by knockdown of PRDX or HO-1 proteins. (A) The measurement of LPO levels in LX-2 cells after treatment with si-*PRDX*s, si-*HO-1* or the negative control si-NC (mean ± SEM, $n = 3$; *$P < 0.05$, **$P < 0.01$ *vs*. si-NC). (B) The measurement of Fe^{2+}/Fe^{3+}, with the treatments similarly to Fig. 8A (mean ± SEM, $n = 3$; *$P < 0.05$, **$P < 0.01$ *vs*. si-NC). (C) The measurement of GSH levels, with the treatments similarly to Fig. 8A (mean ± SEM, $n = 3$; *$P < 0.05$, **$P < 0.01$. si-NC). (D) Immunofluorescence staining of intracellular ROS (green) after treatment with celastrol (1 μmol/L) and/or si-*PRDX1*, si-*PRDX2* (scale bar = 100 μm) and si-*PRDX4*, si-*PRDX6* (scale bar = 50 μm). *P* values are calculated by one-way ANOVA followed by the Tukey's test.

the protein targets of artemisinin[34,52], curcumin[53] and andrographolide[54]. The ABPP result indicates that celastrol can directly bind to several PRDXs and HO-1. Next, pull down−WB, CETSA−WB and immunofluorescence staining experiments all strongly demonstrated that celastrol targets to PRDX family members including PRDX1, PRDX2, PRDX4, and PRDX6, as well as HO-1.

Recently, celastrol was reported to inhibit PRDX2 activity to result in the increase of ROS level, leading to endoplasmic reticulum stress and apoptosis in gastric cancer cells[41]. More recent studies provided evidence about the role of PRDX1 and PRDX6 as negative regulators of ferroptotic cell death[45,55]. Our data show that celastrol causes the disturbance of the ROS, LPO and Fe^{2+}/Fe^{3+} homeostasis to induce the ferroptosis of activated-HSCs, which is at least partly mediated by inhibiting the anti-oxidant activities of PRDXs. Although celastrol does not affect the expression levels of PRDXs *in vivo* and *in vitro*, our data show that the knockdown of PRDXs induces the ferroptosis of HSCs to a certain extent, and more importantly, this could be reversed by either of the two ferroptosis inhibitors DFO and NAC. Although the individual siRNA results in Fig. S11D didn't show statically significant changes of α-SMA protein level, we could not rule out the possibility of protein function redundancy and/or mutual compensation effect especially for these PRDX family

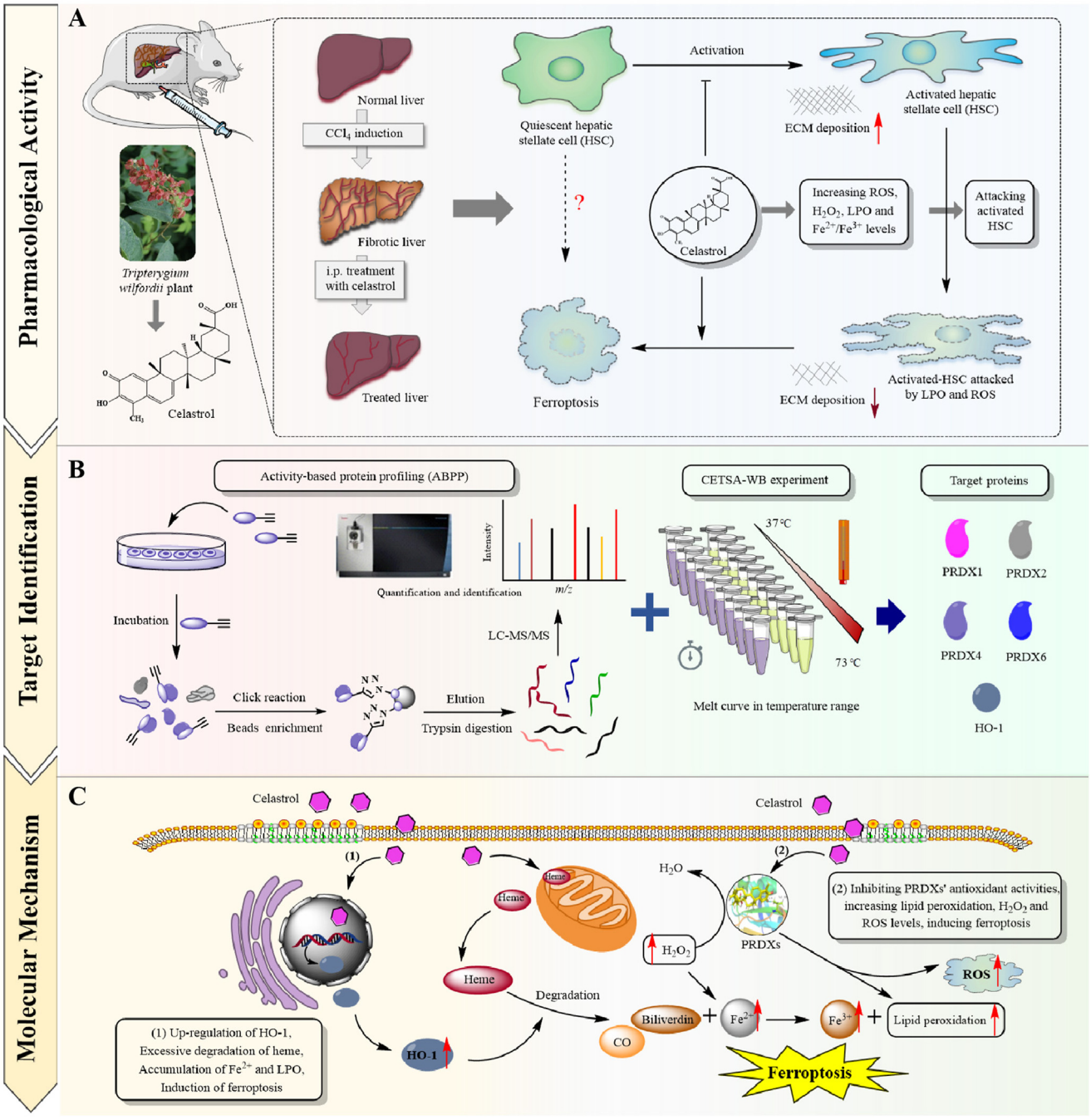

Figure 9 Schematic summary of the study. (A) Celastrol induces the ferroptosis of activated-HSCs to ameliorate hepatic fibrosis. (B) ABPP strategy discovered that celastrol directly targets to PRDXs and HO-1. (C) Celastrol induces the ferroptosis of activated-HSCs *via* regulating HO-1, PRDXs and ROS-mediated processes.

members[56]. In addition, celastrol may exert anti-fibrotic activity *via* targeting other proteins (discussed below).

Celastrol is able to covalently interact with the SH group of protein *via* a Michael addition reaction[47]. Both competition experiments using compounds with known cysteine-binding activities and labeling experiments on the cysteine-mutant proteins were carried out. Our experimental data support that celastrol mainly binds to Cys83 and Cys173 of PRDX1 rather than Cys52 and Cys71 site, in agreement with a previous report for triptolide targeting to PRDX1[57]. Moreover, Cys172 of PRDX2 is discovered as the major binding site of celastrol. Notable, both Cys173 of PRDX1 and Cys172 of PRDX2 are the so-called resolving cysteine, which is necessary for the completion of peroxidatic cycle[58].

In addition to PRDX family, celastrol may exert anti-fibrotic activity *via* targeting other proteins. For instance, the ABPP results indicated that celastrol could also interact with HO-1, high mobility group protein B1 (HMGB1) and voltage-dependent anion channels (VDACs). HO-1 catabolizes the transformation of free heme into Fe^{2+}, biliverdin and CO[59]. HO-1 is closely related to ferroptosis and oxidative stress in the pathological processes of hepatic fibrosis and cancer[21,60]. Although celastrol could partially

inhibit the activity of HO-1 at a higher concentration, it seems mainly working through upregulation of HO-1 *in vivo* and *in vitro*, which may cause the excessive decomposition of heme and the accumulation of Fe^{2+}, which ultimately induces ferroptosis. HMGB1 is an intensively-studied protein as the proinflammatory alarmin or damage-associated molecular pattern molecule[61]. Recent study suggested that it is related to the ferroptosis of mesangial cells when in response to high glucose[62] and we recently reported it as a target of celastrol in cerebral ischemia−reperfusion[33]. VDAC2 and VDAC3 belong to the membrane-spanning channels that facilitate the transport of ions and metabolites across the outer mitochondrial membrane. They are the known targets of erastin, a ferroptosis activator[63,64]. The involvement and function of these potential targets of celastrol in hepatic fibrosis warrants more detailed studies.

In this present study, we have demonstrated that celastrol effectively ameliorates hepatic fibrosis *via* inducing the ferroptosis of activated-HSCs *in vivo* and *in vitro*. We validated that celastrol could directly bind to PRDX1, PRDX2, PRDX4, PRDX6 (but not PRDX3 and PRDX5) and HO-1 proteins in a covalent manner. Interestingly, celastrol can inhibit the enzymatic activities of PRDX proteins *via* modifying their active cysteine sites, without affecting the expressions. Moreover, celastrol up-regulates the expression of HO-1. These lead to the accumulation of LPO, ROS and Fe^{2+} to induce ferroptosis in activated-HSCs.

5. Conclusions

Celastrol can ameliorate hepatic fibrosis *via* targeting PRDXs and HO-1 to induce the ferroptosis of activated-HSCs, providing a promising therapeutic strategy for hepatic fibrosis.

Acknowledgments

This work was supported by the National Key Research and Development Program of China (2020YFA0908000), the Innovation Team and Talents Cultivation Program of National Administration of Traditional Chinese Medicine (ZYYCXTD-C-202002, China), the National Natural Science Foundation of China (81903588, 81803456, 82074098 and 81841001, China) and the Fundamental Research Funds for the Central Public Welfare Research Institutes (ZXKT18003 and ZZ15-YQ-063, China).

Author contributions

Jigang Wang, Han-Ming Shen and Lingyun Dai designed and supervised the project. Piao Luo was responsible for the animal and cell, target identification and protein knockdown experiments, data analysis and figure production. Dandan Liu and Qian Zhang assisted the animal experiment, performed cellular immunostaining. Fan Yang, Yin-Kwan Wong and Chuanbin Yang performed the recombinant protein purification and activity assay. Fei Xia performed probe synthesis. Junzhe Zhang carried out LC−MS/MS experiments. Jiayun Chen conducted MS data analysis. Ya Tian performed molecular docking analysis. Piao Luo drafted the manuscript. Piao Luo, Fan Yang, Qian Zhang, Lingyun Dai and Jigang Wang revised the article. All authors read and approved the manuscript.

Conflicts of interest

The authors declare no conflicts of interest.

Appendix A. Supporting information

Supporting data to this article can be found online at https://doi.org/10.1016/j.apsb.2021.12.007.

References

1. Lim YS, Kim WR. The global impact of hepatic fibrosis and end-stage liver disease. *Clin Liver Dis* 2008;**12**:733−746, vii.
2. Xu R, Zhang Z, Wang FS. Liver fibrosis: mechanisms of immune-mediated liver injury. *Cell Mol Immunol* 2012;**9**:296−301.
3. Ellis EL, Mann DA. Clinical evidence for the regression of liver fibrosis. *J Hepatol* 2012;**56**:1171−80.
4. Bataller R, Brenner DA. Liver fibrosis. *J Clin Invest* 2005;**115**:209−18.
5. Trivedi P, Wang S, Friedman SL. The power of plasticity-metabolic regulation of hepatic stellate cells. *Cell Metab* 2021;**33**:242−57.
6. Friedman SL. Mechanisms of disease: mechanisms of hepatic fibrosis and therapeutic implications. *Nat Clin Pract Gastroenterol Hepatol* 2004;**1**:98−105.
7. Jia Y, Wang F, Guo Q, Li M, Wang L, Zhang Z, et al. Curcumol induces RIPK1/RIPK3 complex-dependent necroptosis *via* JNK1/2-ROS signaling in hepatic stellate cells. *Redox Biol* 2018;**19**:375−87.
8. Zhang Z, Yao Z, Zhao S, Shao J, Chen A, Zhang F, et al. Interaction between autophagy and senescence is required for dihydroartemisinin to alleviate liver fibrosis. *Cell Death Dis* 2017;**8**:e2886.
9. Dixon SJ, Lemberg KM, Lamprecht MR, Skouta R, Zaitsev EM, Gleason CE, et al. Ferroptosis: an iron-dependent form of non-apoptotic cell death. *Cell* 2012;**149**:1060−72.
10. Stockwell BR, Friedmann Angeli JP, Bayir H, Bush AI, Conrad M, Dixon SJ, et al. Ferroptosis: a regulated cell death nexus linking metabolism, redox biology, and disease. *Cell* 2017;**171**:273−85.
11. Han C, Liu Y, Dai R, Ismail N, Su W, Li B. Ferroptosis and its potential role in human diseases. *Front Pharmacol* 2020;**11**:239.
12. Chen X, Kang R, Kroemer G, Tang D. Broadening horizons: the role of ferroptosis in cancer. *Nat Rev Clin Oncol* 2021;**18**:280−96.
13. Sun X, Niu X, Chen R, He W, Chen D, Kang R, et al. Metallothionein-1G facilitates sorafenib resistance through inhibition of ferroptosis. *Hepatology* 2016;**64**:488−500.
14. Li Y, Jin C, Shen M, Wang Z, Tan S, Chen A, et al. Iron regulatory protein 2 is required for artemether-mediated anti-hepatic fibrosis through ferroptosis pathway. *Free Radic Biol Med* 2020;**160**:845−59.
15. Zhang Z, Guo M, Shen M, Kong D, Zhang F, Shao J, et al. The BRD7−P53−SLC25A28 axis regulates ferroptosis in hepatic stellate cells. *Redox Biol* 2020;**36**:101619.
16. Zhang Z, Guo M, Li Y, Shen M, Kong D, Shao J, et al. RNA-binding protein ZFP36/TTP protects against ferroptosis by regulating autophagy signaling pathway in hepatic stellate cells. *Autophagy* 2020;**16**:1482−505.
17. Tsurusaki S, Tsuchiya Y, Koumura T, Nakasone M, Sakamoto T, Matsuoka M, et al. Hepatic ferroptosis plays an important role as the trigger for initiating inflammation in nonalcoholic steatohepatitis. *Cell Death Dis* 2019;**10**:449.
18. Zhang Z, Yao Z, Wang L, Ding H, Shao J, Chen A, et al. Activation of ferritinophagy is required for the RNA-binding protein ELAVL1/HuR to regulate ferroptosis in hepatic stellate cells. *Autophagy* 2018;**14**:2083−103.
19. Li ZJ, Dai HQ, Huang XW, Feng J, Deng JH, Wang ZX, et al. Artesunate synergizes with sorafenib to induce ferroptosis in hepatocellular carcinoma. *Acta Pharmacol Sin* 2021;**42**:301−10.
20. Kong Z, Liu R, Cheng Y. Artesunate alleviates liver fibrosis by regulating ferroptosis signaling pathway. *Biomed Pharmacother* 2019;**109**:2043−53.
21. Sui M, Jiang X, Chen J, Yang H, Zhu Y. Magnesium isoglycyrrhizinate ameliorates liver fibrosis and hepatic stellate cell activation by regulating ferroptosis signaling pathway. *Biomed Pharmacother* 2018;**106**:125−33.

22. Kuo CY, Chiu V, Hsieh PC, Huang CY, Huang SJ, Tzeng IS, et al. Chrysophanol attenuates hepatitis B virus X protein-induced hepatic stellate cell fibrosis by regulating endoplasmic reticulum stress and ferroptosis. *J Pharmacol Sci* 2020;**144**:172−82.
23. Hou W, Liu B, Xu H. Celastrol: progresses in structure−modifications, structure−activity relationships, pharmacology and toxicology. *Eur J Med Chem* 2020;**189**:112081.
24. Xu S, Feng Y, He W, Xu W, Xu W, Yang H, et al. Celastrol in metabolic diseases: progress and application prospects. *Pharmacol Res* 2021;**167**:105572.
25. Liu J, Lee J, Salazar Hernandez MA, Mazitschek R, Ozcan U. Treatment of obesity with celastrol. *Cell* 2015;**161**:999−1011.
26. Corson TW, Crews CM. Molecular understanding and modern application of traditional medicines: triumphs and trials. *Cell* 2007;**130**:769−74.
27. Zhao Q, Liu F, Cheng Y, Xiao XR, Hu DD, Tang YM, et al. Celastrol protects from cholestatic liver injury through modulation of SIRT1−FXR signaling. *Mol Cell Proteomics* 2019;**18**:520−33.
28. Yan CY, Ouyang SH, Wang X, Wu YP, Sun WY, Duan WJ, et al. Celastrol ameliorates propionibacterium acnes/LPS-induced liver damage and MSU-induced gouty arthritis *via* inhibiting K63 deubiquitination of NLRP3. *Phytomedicine* 2021;**80**:153398.
29. Zhao Q, Tang P, Zhang T, Huang JF, Xiao XR, Zhu WF, et al. Celastrol ameliorates acute liver injury through modulation of PPARα. *Biochem Pharmacol* 2020;**178**:114058.
30. Chang W, He W, Li PP, Song SS, Yuan PF, Lu JT, et al. Protective effects of celastrol on diethylnitrosamine-induced hepatocellular carcinoma in rats and its mechanisms. *Eur J Pharmacol* 2016;**784**:173−80.
31. Wang Y, Li C, Gu J, Chen C, Duanmu J, Miao J, et al. Celastrol exerts anti-inflammatory effect in liver fibrosis *via* activation of AMPK−SIRT3 signalling. *J Cell Mol Med* 2020;**24**:941−53.
32. Seki E, de Minicis S, Inokuchi S, Taura K, Miyai K, van Rooijen N, et al. CCR2 promotes hepatic fibrosis in mice. *Hepatology* 2009;**50**:185−97.
33. Liu DD, Luo P, Gu L, Zhang Q, Gao P, Zhu Y, et al. Celastrol exerts a neuroprotective effect by directly binding to HMGB1 protein in cerebral ischemia−reperfusion. *J Neuroinflammation* 2021;**18**:174.
34. Wang J, Zhang CJ, Chia WN, Loh CC, Li Z, Lee YM, et al. Haem-activated promiscuous targeting of artemisinin in *Plasmodium falciparum*. *Nat Commun* 2015;**6**:10111.
35. Wang J, Wong YK, Zhang J, Lee YM, Hua ZC, Shen HM, et al. Drug target identification using an iTRAQ-based quantitative chemical proteomics approach-based on a target profiling study of andrographolide. *Methods Enzymol* 2017;**586**:291−309.
36. Yu G, Wang LG, Han Y, He QY. clusterProfiler: an R package for comparing biological themes among gene clusters. *OMICS* 2012;**16**:284−7.
37. Dai L, Zhao T, Bisteau X, Sun W, Prabhu N, Lim YT, et al. Modulation of protein-interaction states through the cell cycle. *Cell* 2018;**173**:1481−1494 e13.
38. Jafari R, Almqvist H, Axelsson H, Ignatushchenko M, Lundbäck T, Nordlund P, et al. The cellular thermal shift assay for evaluating drug target interactions in cells. *Nat Protoc* 2014;**9**:2100−22.
39. Trott O, Olson AJ. AutoDock Vina: improving the speed and accuracy of docking with a new scoring function, efficient optimization, and multithreading. *J Comput Chem* 2010;**31**:455−61.
40. Liu CX, Yin QQ, Zhou HC, Wu YL, Pu JX, Xia L, et al. Adenanthin targets peroxiredoxin I and II to induce differentiation of leukemic cells. *Nat Chem Biol* 2012;**8**:486−93.
41. Chen X, Zhao Y, Luo W, Chen S, Lin F, Zhang X, et al. Celastrol induces ROS-mediated apoptosis *via* directly targeting peroxiredoxin-2 in gastric cancer cells. *Theranostics* 2020;**10**:10290−308.
42. Mucha O, Podkalicka P, Mikulski M, Barwacz S, Andrysiak K, Biela A, et al. Development and characterization of a new inhibitor of heme oxygenase activity for cancer treatment. *Arch Biochem Biophys* 2019;**671**:130−42.
43. Rhee SG, Kang SW, Chang TS, Jeong W, Kim K. Peroxiredoxin, a novel family of peroxidases. *IUBMB Life* 2001;**52**:35−41.
44. Rhee SG, Chae HZ, Kim K. Peroxiredoxins: a historical overview and speculative preview of novel mechanisms and emerging concepts in cell signaling. *Free Radic Biol Med* 2005;**38**:1543−52.
45. Lu B, Chen XB, Hong YC, Zhu H, He QJ, Yang B, et al. Identification of PRDX6 as a regulator of ferroptosis. *Acta Pharmacol Sin* 2019;**40**:1334−42.
46. Abo M, Li C, Weerapana E. Isotopically-labeled iodoacetamide-alkyne probes for quantitative cysteine-reactivity profiling. *Mol Pharm* 2018;**15**:743−9.
47. Zhang D, Chen Z, Hu C, Yan S, Li Z, Lian B, et al. Celastrol binds to its target protein *via* specific noncovalent interactions and reversible covalent bonds. *Chem Commun (Camb)* 2018;**54**:12871−4.
48. Pradhan-Sundd T, Zhou L, Vats R, Jiang A, Molina L, Singh S, et al. Dual catenin loss in murine liver causes tight junctional deregulation and progressive intrahepatic cholestasis. *Hepatology* 2018;**67**:2320−37.
49. Garcia-Tsao G, Abraldes JG, Berzigotti A, Bosch J. Portal hypertensive bleeding in cirrhosis: risk stratification, diagnosis, and management: 2016 practice guidance by the American Association for the study of liver diseases. *Hepatology* 2017;**65**:310−35.
50. Tomita K, Teratani T, Suzuki T, Shimizu M, Sato H, Narimatsu K, et al. Free cholesterol accumulation in hepatic stellate cells: mechanism of liver fibrosis aggravation in nonalcoholic steatohepatitis in mice. *Hepatology* 2014;**59**:154−69.
51. Bian M, Chen X, Zhang C, Jin H, Wang F, Shao J, et al. Magnesium isoglycyrrhizinate promotes the activated hepatic stellate cells apoptosis *via* endoplasmic reticulum stress and ameliorates fibrogenesis *in vitro* and *in vivo*. *Biofactors* 2017;**43**:836−46.
52. Zhang J, Sun X, Wang L, Wong YK, Lee YM, Zhou C, et al. Artesunate-induced mitophagy alters cellular redox status. *Redox Biol* 2018;**19**:263−73.
53. Wang J, Zhang J, Zhang CJ, Wong YK, Lim TK, Hua ZC, et al. *In situ* proteomic profiling of curcumin targets in HCT116 colon cancer cell line. *Sci Rep* 2016;**6**:22146.
54. Wang J, Tan XF, Nguyen VS, Yang P, Zhou J, Gao M, et al. A quantitative chemical proteomics approach to profile the specific cellular targets of andrographolide, a promising anticancer agent that suppresses tumor metastasis. *Mol Cell Proteomics* 2014;**13**:876−86.
55. Lovatt M, Adnan K, Kocaba V, Dirisamer M, Peh GSL, Mehta JS. Peroxiredoxin-1 regulates lipid peroxidation in corneal endothelial cells. *Redox Biol* 2020;**30**:101417.
56. Knaus UG. Oxidants in physiological processes. In: Schmidt HHHW, Ghezzi P, Cuadrado A, editors. *Reactive oxygen species: network pharmacology and therapeutic applications*. Cham: Springer International Publishing; 2021. p. 27−47.
57. Zhao Q, Ding Y, Deng Z, Lee OY, Gao P, Chen P, et al. Natural products triptolide, celastrol, and withaferin A inhibit the chaperone activity of peroxiredoxin I. *Chem Sci* 2015;**6**:4124−30.
58. Wood ZA, Poole LB, Karplus PA. Peroxiredoxin evolution and the regulation of hydrogen peroxide signaling. *Science* 2003;**300**:650−3.
59. Gozzelino R, Jeney V, Soares MP. Mechanisms of cell protection by heme oxygenase-1. *Annu Rev Pharmacol Toxicol* 2010;**50**:323−54.
60. Chiang SK, Chen SE, Chang LC. A dual role of heme oxygenase-1 in cancer cells. *Int J Mol Sci* 2018;**20**:39.
61. Yang H, Antoine DJ, Andersson U, Tracey KJ. The many faces of HMGB1: molecular structure−functional activity in inflammation, apoptosis, and chemotaxis. *J Leukoc Biol* 2013;**93**:865−73.
62. Wu Y, Zhao Y, Yang HZ, Wang YJ, Chen Y. HMGB1 regulates ferroptosis through Nrf2 pathway in mesangial cells in response to high glucose. *Biosci Rep* 2021;**41**:BSR20202924.
63. Yagoda N, von Rechenberg M, Zaganjor E, Bauer AJ, Yang WS, Fridman DJ, et al. RAS−RAF−MEK-dependent oxidative cell death involving voltage-dependent anion channels. *Nature* 2007;**447**:864−8.
64. Yang Y, Luo M, Zhang K, Zhang J, Gao T, Connell DO, et al. Nedd4 ubiquitylates VDAC2/3 to suppress erastin-induced ferroptosis in melanoma. *Nat Commun* 2020;**11**:433.